Isotropic in-plane quenched disorder and dilution induce a robust nematic state in electron-doped pnictides

Shuhua Liang,[1,2] Christopher B. Bishop,[1,2] Adriana Moreo,[1,2] and Elbio Dagotto[1,2]
[1]*Department of Physics and Astronomy,University of Tennessee, Knoxville, Tennessee 37966, USA*
[2]*Materials Science and Technology Division, Oak Ridge National Laboratory,Oak Ridge, Tennessee 37831, USA*
(Received 28 May 2015; revised manuscript received 2 August 2015; published 21 September 2015)

The phase diagram of electron-doped pnictides is studied varying the temperature, electronic density, and isotropic in-plane quenched disorder strength and dilution by means of computational techniques applied to a three-orbital (xz,yz,xy) spin-fermion model with lattice degrees of freedom. In experiments, chemical doping introduces disorder but in theoretical studies the relationship between electronic doping and the randomly located dopants, with their associated quenched disorder, is difficult to address. In this publication, the use of computational techniques allows us to study independently the effects of electronic doping, regulated by a global chemical potential, and impurity disorder at randomly selected sites. Surprisingly, our Monte Carlo simulations reveal that the fast reduction with doping of the Néel T_N and the structural T_S transition temperatures, and the concomitant stabilization of a robust nematic state, is primarily controlled in our model by the magnetic dilution associated with the in-plane isotropic disorder introduced by Fe substitution. In the doping range studied, changes in the Fermi surface produced by electron doping affect only slightly both critical temperatures. Our results also suggest that the specific material-dependent phase diagrams experimentally observed could be explained as a consequence of the variation in disorder profiles introduced by the different dopants. Our findings are also compatible with neutron scattering and scanning tunneling microscopy, unveiling a patchy network of locally magnetically ordered clusters with anisotropic shapes, even though the quenched disorder is locally isotropic. This study reveals a remarkable and unexpected degree of complexity in pnictides: the fragile tendency to nematicity intrinsic of translational invariant electronic systems needs to be supplemented by quenched disorder and dilution to stabilize the robust nematic phase experimentally found in electron-doped 122 compounds.

DOI: 10.1103/PhysRevB.92.104512 PACS number(s): 74.70.Xa, 74.25.Dw, 71.10.Fd

I. INTRODUCTION

The mechanism that leads to high critical temperature superconductivity in iron pnictides [1–5] is still elusive, mainly because the several simultaneously active degrees of freedom (d.o.f.) in these materials pose a major theoretical challenge. While magnetic mechanisms are often invoked to explain the d-wave superconductivity in cuprates [6,7], the role of the orbitals is added to the mix in the case of the iron-based compounds. Moreover, the symmetry of their superconducting state is still under considerable debate [8].

The interaction among the many different d.o.f. in pnictides generates rich phase diagrams when varying temperature and doping [9]. In addition to the superconducting phase, magnetic and nematic phases, accompanied by structural distortions, have been identified [9–13]. To properly address this difficult problem, it is necessary that the spin, orbital, lattice, and charge should all be incorporated in a treatable model that allows to monitor their respective roles in the properties of these materials. Due to the complexity of the problem, most of the previous theoretical studies have been performed either in the weak or strong coupling limits. In weak coupling, the interactions among the electrons are considered small and the physical properties are studied in momentum space in terms of itinerant electrons, with emphasis on the particular properties of their Fermi surfaces (FS) such as nesting [14–17]. On the other hand, the strong coupling approach is based on the experimental observation of localized magnetic moments and on the fact that several properties of the pnictides can be reproduced via Heisenberg models [18–20]. Both approaches were successful in the study of the magnetic properties of the parent compounds, indicating that in these materials both localized and itinerant magnetic moments are important. However, upon doping, there are challenges explaining experimental data in both approximations. In particular, when doping is achieved by chemical substitution of iron atoms, then the effects of disorder and dilution must also be incorporated into the theoretical considerations.

The parent compound of the 122 family, $BaFe_2As_2$, can be doped with electrons by replacing Fe by a transition metal (TM) resulting in $Ba(Fe_{1-x}TM_x)_2As_2$ or with holes by replacing Ba by an alkali metal (A) leading to $Ba_{1-x}A_xFe_2As_2$ [8]. It is also possible to dope in an isovalent manner replacing, for example, Fe with Ru to obtain $Ba(Fe_{1-x}Ru_x)_2As_2$ [21]. Nominally, replacing Fe with Ru, Co, Ni, and Cu would introduce 0, 1, 2, and 3 electrons per dopant atom. However, experiments indicate a difference between nominal doping x and the measured doping concentration x_m usually determined using wavelength dispersive x-ray spectroscopy (WDS) [9]. This means that in some cases, electrons can get trapped by the doped impurities [22]. Chemical substitution introduces an amount of disorder that is difficult to control experimentally. In addition to electrons being trapped, other effects such as magnetic dilution and impurity scattering may also occur [23].

In undoped 122 compounds, the structural and the Néel transition temperatures, T_S and T_N, are equal to each other. Upon electron doping, both are rapidly reduced, with T_S decreasing at an equal or slower rate than T_N [9,21]. The reduction of these temperatures is explained in weak coupling by a loss of FS nesting induced by the electronic doping and in strong coupling by magnetic dilution as in t-J models. However, these views seem to be in contradiction with several

experimental results. For example, in $Ba(Fe_{1-x}Ru_x)_2As_2$, which nominally does not introduce electronic doping, and associated changes in FS should not be expected, both T_S and T_N decrease with doping and the material eventually becomes superconducting [21]. In addition, doping with Co, Ni, and Cu is expected to introduce 1, 2, and 3 extra electrons per doped atom. However, the experimentally observed reduction on T_N and T_S was found to be primarily a function of the doping x rather than of the density of electrons [9,24]. Experiments, thus, indicate that when dopants are introduced directly on the Fe-As planes, as it is the case for electron-doped 122 materials, disorder and dilution must play an important role [9,17,25–30]. Due to the experimental uncertainty on the doping concentration and the nature of the disorder, a theoretical understanding of the phase diagrams under these challenging circumstances is elusive. Density functional theory (DFT) studies indicated that in-plane-doped atoms would tend to trap electrons [22], while first-principles methods found that the interplay between on-site and off-site impurity potentials could induce FS distortions in nominally isovalent doping [23]. Moreover, a calculation considering two-orbiton processes predicts a nonsymmetric impurity potential which could be responsible for the observed transport anisotropies [17].

In this publication, the effects of electron doping in the 122 pnictides will be studied numerically using a spin-fermion model (SFM) for the pnictides [31–33] including the lattice d.o.f. [34]. The SFM considers phenomenologically the experimentally motivated evidence that requires a combination of itinerant and localized d.o.f. to properly address the iron-based superconductors [4,5,35,36]. The itinerant sector mainly involves electrons in the xz, yz, and xy d orbitals [37] while the localized spins represent the spin of the other d orbitals [31,32], or in a Landau-Ginzburg context it can be considered as the magnetic order parameter.

The focus of this effort will be on the structural and the Néel transitions, and the properties of the resulting nematic phase that will be monitored as a function of the electronic and impurity densities. Earlier studies performed in the undoped parent compounds indicated that the coupling between the lattice orthorhombic distortion $\epsilon_{\mathbf{i}}$, associated to the elastic constant C_{66}, and the spin-nematic order parameter $\Psi_{\mathbf{i}}$ stabilizes the orthorhombic $(\pi,0)$ antiferromagnetic (AFM) ground state [34] with $T_S = T_N$ as in the 122 materials [9]. The small separation between T_S and T_N observed in the parent compounds of the 1111 family [38] was found to be regulated by the coupling of the lattice orthorhombic distortion to the orbital order parameter $\Phi_{\mathbf{i}}$ [34].

The effect of disorder in iron superconductors has been studied before using mainly analytical or semianalytical techniques and primarily in the context of Fermi surface nesting (for a partial list of references see Refs. [39,40]). However, ours is the first time that electronic doping supplemented by quenched disorder and dilution effects is computationally studied in a system that includes magnetic, charge, orbital, and lattice d.o.f. Our numerical approach involves Monte Carlo (MC) calculations on the localized spin and lattice components, combined with a fermionic diagonalization of the charge/orbital sector. Technically, we also employ twisted boundary conditions (TBC) and the travelling cluster approximation (TCA) is implemented [41] in order to study large clusters of size 64×64, a record for the spin-fermion model. This numerical approach allows us to incorporate the effects of in-plane chemical doping and to gather results for temperatures above T_S where all d.o.f. develop strong short-range fluctuations [14,42], a difficult regime for other many-body procedures. Our main conclusion is that disorder and dilution are needed to stabilize the broad nematic phase in 122 materials observed experimentally. That a critical temperature such as T_N decreases faster with doping by including disorder than in the clean limit is natural [43,44], but our most novel result is the concomitant stabilization of a nematic regime. In other words, T_N and T_S are affected *differently* by disorder/dilution. Isotropic dopant profiles are sufficient to obtain these results. Our analysis illustrates the interdependence of the many degrees of freedom present in real materials and the need to study models with robust many-body techniques to unveil the physics that emerges in these complex systems.

The organization of the paper is as follows: the model is described in Sec. II and the computational methods are presented in Sec. III. Section IV is devoted to the main results addressing the phase diagram upon doping. Section V describes the properties of the nematic phase stabilized in our study, including a comparison with neutron scattering and scanning tunneling microscopy experiments. The discussion and summary are the scope of Sec. VI.

II. MODEL

A. Hamiltonian

The spin-fermion model Hamiltonian studied here is based on the original purely electronic model [31–33] supplemented by the recent addition of couplings to the lattice degrees of freedom [41]:

$$H_{\mathrm{SF}} = H_{\mathrm{Hopp}} + H_{\mathrm{Hund}} + H_{\mathrm{Heis}} + H_{\mathrm{SL}} + H_{\mathrm{Stiff}}. \qquad (1)$$

H_{Hopp} is the three-orbitals (d_{xz}, d_{yz}, d_{xy}) tight-binding Fe-Fe hopping of electrons, with the hopping amplitudes selected to reproduce ARPES experiments. Readers can find these amplitudes in previous publications, such as in Eqs. (1)– (3) and Table 1 of Ref. [37]. The average density of electrons per iron and per orbital is $n = 4/3$ in the undoped limit [37] and its value in the doped case is controlled via a chemical potential included in H_{Hopp} [41]. The Hund interaction is standard: $H_{\mathrm{Hund}} = -J_{\mathrm{H}} \sum_{\mathbf{i},\alpha} \mathbf{S_i} \cdot \mathbf{s}_{\mathbf{i},\alpha}$, with $\mathbf{S_i}$ the localized spin at site $\mathbf{i}$ (with magnitude 1) and $\mathbf{s}_{\mathbf{i},\alpha}$ the itinerant spin corresponding to orbital α at the same site [45]. H_{Heis} contains the Heisenberg interaction among the localized spins involving both nearest neighbors (NN) and next-NN (NNN) interactions with respective couplings J_{NN} and J_{NNN}, and a ratio $J_{\mathrm{NNN}}/J_{\mathrm{NN}} = 2/3$ (any ratio larger than $1/2$ would have been equally effective to favor "striped" spin order). For specific details, see Sec. III below. Having NN and NNN Heisenberg interactions of comparable magnitude arise from having comparable NN and NNN hoppings, caused by the geometry of the material.

The coupling between the spin and lattice degrees of freedom is given by $H_{\mathrm{SL}} = -g \sum_{\mathbf{i}} \Psi_{\mathbf{i}} \epsilon_{\mathbf{i}}$ [15,16], where g is the spin-lattice coupling [46]. The spin nematic order parameter

is defined as

$$\Psi_{\mathbf{i}} = \mathbf{S_i} \cdot \mathbf{S_{i+y}} - \mathbf{S_i S_{i+x}}, \tag{2}$$

where $\mathbf{x}$ and $\mathbf{y}$ are unit vectors along the x and y axes, respectively. This order parameter becomes 2 in the perfect $(\pi,0)$ state. The lattice $\epsilon_{\mathbf{i}}$ degree of freedom related to the tetragonal to orthorhombic distortion has a more complex definition in terms of the positions of the As or Se atoms, and its precise definition can be found in Ref. [34]. $H_{\rm Stiff}$ is the lattice stiffness given by a Lennard-Jones potential that speeds up convergence, as previously discussed [41].

Note that the lattice-orbital coupling term, $H_{\rm OL} = -\lambda \sum_{\mathbf{i}} \Phi_{\mathbf{i}} \epsilon_{\mathbf{i}}$ [41], with the orbital nematic order parameter defined as

$$\Phi_{\mathbf{i}} = n_{\mathbf{i},\rm xz} - n_{\mathbf{i},\rm yz}, \tag{3}$$

where $n_{\rm xz}$ and $n_{\rm yz}$ are the number operators for the orbitals indicated, is omitted because previous work indicated that λ induces a (small) nematic phase with $T_S > T_N$ directly in the parent compounds [34,41]. Since the goal of the present effort is to study the 122 family, characterized by $T_S = T_N$ in the undoped case, then this term is not included to reduce the number of parameters.

We also wish to clarify that when varying the global chemical potential, thus modifying the electronic density, we assume that all couplings are unaffected. In particular, since the orbitals that induce the localized spins are assumed to be weakly affected by modifications in the position of the Fermi level, then there is no obvious reason to modify $J_{\rm NN}$ and $J_{\rm NNN}$ with increasing electron doping. This is similar as in studies of manganites via the double-exchange model where with doping the couplings of the t_{2g} sector are assumed to be fixed [47].

B. Quenched disorder and dilution

On-site diagonal disorder is introduced by adding an impurity potential $I_I(\mathbf{i}_d)$ to N_I randomly selected sites $\mathbf{i}_d$ where transition metal atoms replace Fe. The density of impurity atoms x is defined as $x = N_{\rm I}/N$, where N is the total number of lattice sites. In addition, the value of the localized spin at the impurity site, S_I, is reduced since, for example, Co dopants in $BaFe_2As_2$ are nonmagnetic [48]. This effectively reduces the local Hund coupling $J_{\rm H,I}$ and the spin-lattice coupling $g_{\rm I}$ at the impurity sites. We also will study the effect of extending the spatial range of the impurity by reducing the values of the localized spins to $S_{\rm NN}$ ($S_{\rm NNN}$) at the NN (NNN) of the impurity sites with the corresponding effective decrease in $J_{\rm H}$ and g at those sites (see Fig. 1). Thus off-diagonal isotropic disorder results from the effective reduction of the Heisenberg couplings at the bonds connecting the impurity sites and their neighbors [45]. Note that off-diagonal disorder could also be introduced in the eight hopping amplitudes present in $H_{\rm Hopp}$ [41] but for simplicity we decided not to consider hopping disorder at this time.

III. METHODS

The Hamiltonian in Eq. (1) was studied via a well-known Monte Carlo method [33,47] applied to (i) the localized (assumed classical) spin degrees of freedom $\mathbf{S_i}$ and (ii) the atomic

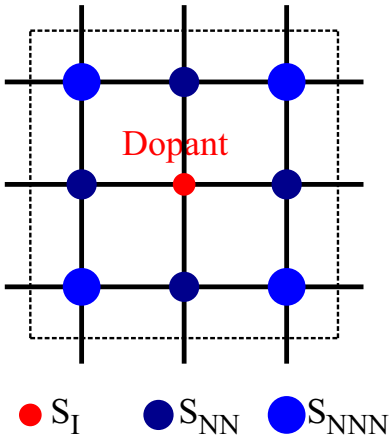

FIG. 1. (Color online) Internal structure of dopant sites. Sketch shows the location of a dopant where the magnitude of the localized spin, $S_{\rm I}$, is reduced from the original value S. In addition, the neighboring localized spins are also assumed to be affected by the presence of the dopant. The four immediate nearest neighbors have a new localized spin magnitude $S_{\rm NN}$, while the four next-nearest neighbors have a new localized spin magnitude $S_{\rm NNN}$, such that $S_{\rm I} \leqslant S_{\rm NN} \leqslant S_{\rm NNN} \leqslant S$ (S is the undoped localized spin magnitude, assumed to be 1 in this publication unless otherwise stated).

displacements that determine the local orthorhombic lattice distortion $\epsilon_{\mathbf{i}}$ [34,41]. For each Monte Carlo configuration of spins and atomic positions, the remaining quantum fermionic Hamiltonian is diagonalized. The simulations are performed at various temperatures, dopings, and disorder configurations and local and long-range observables are measured. Note that with the exact diagonalization technique results can be obtained comfortably only on up to 8×8 lattices, which may be too small to provide meaningful data at the low rates of doping relevant in the pnictides. For this reason, we have also used the traveling cluster approximation [49] where a larger lattice (64×64 sites in most of this effort) can be studied by performing the MC updates via a travelling cluster centered at consecutive sites $\mathbf{i}$, with a size substantially smaller than the full lattice size of the entire system. Twisted boundary conditions were also used [50] to obtain (almost) a continuum range of momenta. For simplicity, most couplings are fixed to values used successfully before [33]: $J_{\rm H} = 0.1$ eV, $J_{\rm NN} = 0.012$ eV, and $J_{\rm NNN} = 0.008$ eV. The dimensionless version of the spin-lattice coupling $\tilde{g}$ is fixed to 0.16 as in Ref. [34]. The focus of the publication is on the values for the parameters associated with disorder and the corresponding physical results, as discussed in the sections below.

An important technical detail is that to improve numerical convergence, and to better mimic real materials that often display an easy-axis direction for spin orientation, we have introduced a small anisotropy in the x component of the superexchange interaction so that the actual Heisenberg interaction is

$$H_{\rm Heis} = J_{\rm NN} \sum_{\langle \mathbf{ij} \rangle} \left(\mathbf{S_i} \cdot \mathbf{S_j} + \delta S_{\mathbf{i}}^x S_{\mathbf{j}}^x \right) + J_{\rm NNN} \sum_{\langle\langle \mathbf{im} \rangle\rangle} \left(\mathbf{S_i} \cdot \mathbf{S_m} + \delta S_{\mathbf{i}}^x S_{\mathbf{m}}^x \right), \tag{4}$$

with $\delta = 0.1$. This anisotropy slightly raises T_N, but the magnetic susceptibility χ_S becomes much sharper at the transition temperatures, facilitating an accurate determination of T_N. It is important to clarify that the easy-axis anisotropy affects the direction in which the spins order, but by no means breaks explicitly the C_4 lattice rotational invariance that is related to nematicity via its spontaneous breaking. In other words, we have checked explicitly that perfect $(\pi,0)$ and $(0,\pi)$ localized spins configurations have identical energy if their spins are oriented along the same axis, either the easy axis, which minimizes the global energy or any other. Of course if, say, $(\pi,0)$ is oriented along the x axis and $(0,\pi)$ along the z axis then there is an energy difference, but as long as the spin orientations are the same then the expected degeneracies are present. In fact, previously theoretical studies of nematicity have been performed even in the extreme Ising limit [51].

The Monte Carlo simulations with the TCA procedure were mainly performed using 64×64 square lattices [52]. Typically 5000 MC steps were devoted to thermalization and 10 000 to 25 000 steps for measurements at each temperature, doping, and disorder configuration. The results presented below arise from averages over five different disorder configurations. The expectation values of observables remain stable upon the addition of extra configurations due to self-averaging. The magnetic transition was determined by the behavior of the magnetic susceptibility defined as

$$\chi_{S(\pi,0)} = N\beta\langle S(\pi,0) - \langle S(\pi,0)\rangle\rangle^2, \quad (5)$$

where $\beta = 1/k_B T$, N is the number of lattice sites, and $S(\pi,0)$ is the magnetic structure factor at wave vector $(\pi,0)$ obtained via the Fourier transform of the real-space spin-spin correlations measured in the MC simulations. The structural transition is determined by the behavior of the lattice susceptibility defined by

$$\chi_\delta = N\beta\langle \delta - \langle\delta\rangle\rangle^2, \quad (6)$$

where $\delta = \frac{(a_x - a_y)}{(a_x + a_y)}$, and a_i is the lattice constant along the $i = x$ or y directions. These lattice constants are determined from the orthorhombic displacements $\epsilon_{\mathbf{i}}$ [41].

IV. RESULTS

Our first task is to understand the effect of doping and disorder on the magnetic and structural transitions. For this purpose, we studied the evolution of T_N and T_S versus doping concentration under different disorder setups.

A. Clean limit

Consider first the "clean limit." The red squares in Fig. 2 show the evolution of T_N and T_S when the electronic doping does *not* introduce disorder. In this case, T_N is hardly affected and it continues to be equal to T_S for all dopings investigated here. This result indicates that the reduction of T_N and T_S, and the stabilization of a nematic phase in between the two transitions observed experimentally upon electron doping [9], does not emerge just from the reduction of FS nesting induced by the electronic doping. This conclusion is not surprising if we recall that the undoped N-site lattice has $4N$ electrons which means that for $x = 10\%$ the number of added electrons is $N_e = 0.1N$ and, thus, the percentual change in the electronic density is just $100 \times (0.1N/4N) = 2.5\%$. Such a small percentual variation in the electronic density should not produce substantial modifications in the FS, explaining why the changes in nesting are small and, thus, why the critical temperatures are not significantly affected. In fact, we have calculated explicitly the FS and confirmed that it hardly changes in the range of doping studied and in the clean limit. Then, disorder and dilution are needed to understand the experiments within the context of the spin fermion model.

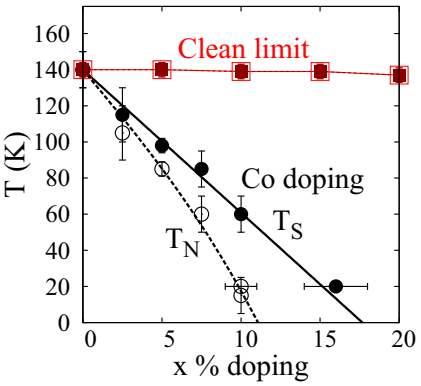

FIG. 2. (Color online) Clean limit and effect of Co doping. The clean limit results (open and solid red points) indicate that $T_S = T_N$ and both are approximately constant in the range studied. For Co doping, the Néel temperature T_N (open circles and black dashed line) and the structural transition temperature T_S (filled circles and black solid line) vs the percentage of impurities x are shown. The on-site disorder is $I_{\mathrm{I}} = -0.1$ and the off-diagonal disorder is determined by $S_{\mathrm{I}} = 0$, $S_{\mathrm{NN}} = S/4$, and $S_{\mathrm{NNN}} = S/2$. For both sets of curves, i.e., with and without quenched disorder, the density of doped electrons equals x to simulate Co doping. The cluster used has a size 64×64.

B. Co doping

To study the effect of quenched disorder, let us first focus on Co doping, which nominally introduces one extra electron per dopant. In Fig. 2, the Néel and structural transition temperatures are presented for the case where one extra electron is contributed by each replaced iron atom, which means that $x = n$, where n is the density of added electrons and x is the density of replaced iron atoms. We considered several possible values for the on-site impurity potential and spin values near the impurity (see details discussed below) and we found that the experimental data of Ref. [9] were best reproduced by setting the on-site impurity potential as $I_{\mathrm{I}} = -0.1$ (in eV units) [53] and by using $S_{\mathrm{I}} = 0$ at the impurities since there is evidence that Co doped in $BaFe_2As_2$ is nonmagnetic [48]. This effectively sets to zero the Hund coupling $J_{\mathrm{H,I}}$ and the spin-lattice coupling g_{I} at the impurity sites. In addition, we also reduced the localized spins to $S/4$ ($S/2$) at the NN (NNN) of the impurity sites with the corresponding effective decreased in J_{H} and g at those sites. The overall chemical potential μ was adjusted so that the density of added impurities equals the density of added electrons, which corresponds to an ideal Co doping [9].

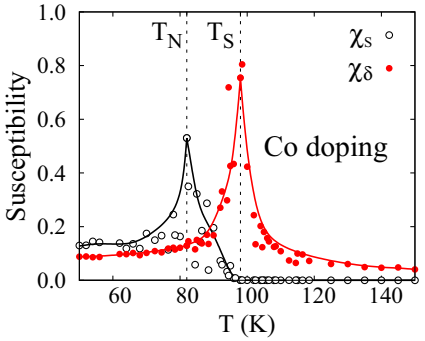

FIG. 3. (Color online) The magnetic susceptibility (open black symbols) and the lattice susceptibility (filled red symbols) vs temperature. The sharp peaks indicate the Néel temperature T_N and the structural transition temperature T_S for the case of 5% Co doping. The on-site disorder is $I_{\rm I} = -0.1$ and the off-diagonal disorder is defined by $S_{\rm I} = 0$, $S_{\rm NN} = S/4$, and $S_{\rm NNN} = S/2$. The cluster used is 64×64.

The black filled (open) circles in Fig. 2 show the evolution with impurity doping of the structural (Néel) transition temperatures in the presence of the disorder caused by replacing Fe by Co at random sites. The magnetic dilution induced by doping causes a rapid reduction in T_S and T_N, similarly as observed in experiments [9], and remarkably also opens a robust nematic phase for $T_N < T < T_S$ since disorder affects *differently* both transition temperatures. In fact, the separation between T_N and T_S is very clear in the magnetic and lattice susceptibilities that are displayed for 5% doping, as example, in Fig. 3. The magnetic properties of the different phases are also clear by monitoring the behavior of the real-space spin-spin correlation functions presented in Fig. 4. In panel (a) for $T = 120$ K ($T > T_S$), the spin correlations effectively

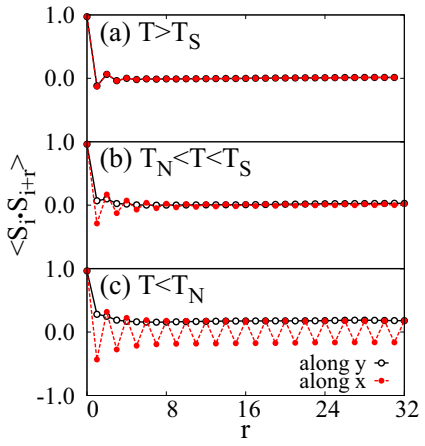

FIG. 4. (Color online) Real-space spin-spin correlation functions vs distance on a 64×64 lattice; (a) corresponds to $T = 120$ K ($T > T_S$) in the paramagnetic regime, (b) to $T = 95$ K ($T_N < T < T_S$) in the nematic state, and (c) to $T = 80$ K ($T < T_N$) in the long-range ordered magnetic state. The AFM correlations along x are indicated with solid circles while the FM correlations along y are denoted with open circles. The results are for 5% Co doping with off-diagonal disorder set by $S_{\rm I} = 0$, $S_{\rm NN} = S/4$, and $S_{\rm NNN} = S/2$.

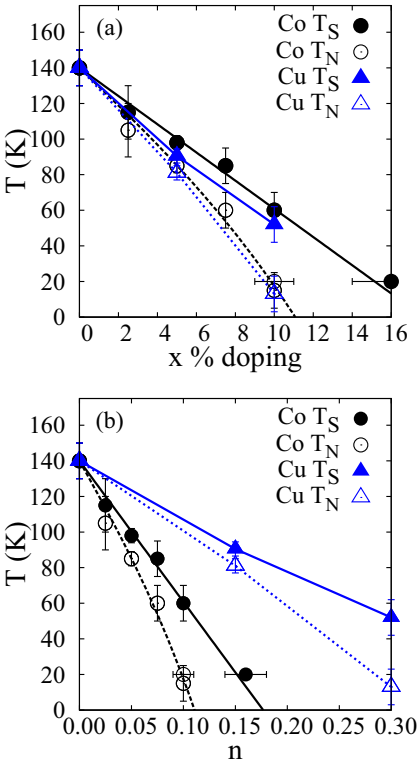

FIG. 5. (Color online) Contrast of effects of Cu and Co doping. The Néel temperatures T_N (dashed lines) and the structural transition temperatures T_S (solid lines) for Co doping (black open and solid circles) and for Cu doping (blue open and solid triangles) are shown. Results are presented first (a) vs the impurity density x and second (b) vs the added electronic density n. The off-diagonal disorder is set at $S_{\rm I} = 0$, $S_{\rm NN} = S/4$, and $S_{\rm NNN} = S/2$. The cluster size is 64×64.

vanish at distances larger than two lattice constants and there is no difference between the results along the x and y axes directions, indicating a paramagnetic ground state. However, at $T = 95$ K ($T_N < T < T_S$), panel (b), the correlations now display short-range AFM (FM) order along the x (y) directions demonstrating the breakdown of the rotational invariance that characterizes the nematic phase, but without developing long-range order as expected. Lowering the temperature to $T = 80$ K ($T < T_N$), panel (c), now the correlations have developed long-range $(\pi,0)$ order, as expected in the antiferromagnetic ground state. To our knowledge, the results in figures such as Fig. 2 provide the largest separation between T_S and T_N ever reported in numerical simulations of realistic models for iron-based superconductors.

C. Cu doping

Let us consider now the effect of doping with Cu which, nominally, introduces three electrons per doped impurity [9]. For this purpose, we increased the chemical potential at a faster rate so that the added density of electrons is $n = 3x$, instead of $n = x$ as for Co doping. The results are shown in Fig. 5. When the critical temperatures for both Cu and Co doping are plotted as a function of the density of impurities x, in Fig. 5(a) it can be seen that the results are approximately *independent* of the kind of dopant. This indicates that the

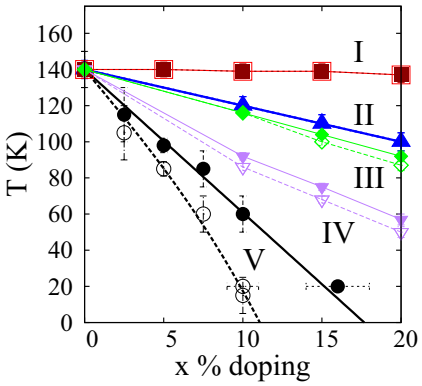

FIG. 6. (Color online) Dependence of results with impurity characteristics. The Néel transition temperature T_N (dashed lines) and the structural transition temperature T_S (solid lines) vs the percentage of impurities x for different settings of the off-diagonal disorder. Case I corresponds to the clean limit with no impurity sites (red squares). Case II has $S_I = S/2$ and $S_{NN} = S_{NNN} = S$ untouched (blue triangles). This case may be sufficient for Ru doping, which is magnetic. Case III has $S_I = 0$ and $S_{NN} = S_{NNN} = S$ untouched (green diamonds). Case IV has $S_I = S/2$, $S_{NN} = 0.7S$, and $S_{NNN} = 0.9S$ (purple upside-down triangles). Finally, Case V has $S_I = 0$, $S_{NN} = S/4$, and $S_{NNN} = S/2$ (black circles). Case V appears to be the best to describe experiments for nonmagnetic doping. The density of doped electrons equals x as in Co doping. In all cases, the on-site disorder potential is kept fixed at $I_I = -0.1$. The lattice size is 64×64.

critical temperatures are primarily controlled by the amount of quenched disorder (namely, by the number of impurity sites) rather than by the actual overall electronic density, at least in the range studied. This conclusion is in excellent agreement with the experimental phase diagrams shown, for example, in Fig. 26(a) of Ref. [9], for the case of several transition metal oxide dopants. Thus, working at a fixed electronic density n, the values of T_N and T_S are smaller for the case of Co doping than for the case of Cu-doping, as shown in Fig. 5(b), because more Co than Cu impurities have to be added to achieve the same electronic density, underlying the fact that Co doping introduces more disorder than Cu doping at fixed n. These results are also in good agreement with the experimental phase diagram in Fig. 26(b) of Ref. [9].

D. Dependence on impurity characteristics

Let us consider the dependence of the Néel and the structural transitions temperatures on the local details of the magnetic dilution caused by the disorder. In Fig. 6, results for T_N and T_S are shown as a function of impurity doping with the chemical potential set to introduce one electron per dopant. The clean limit data (red squares, case I) is displayed again for the sake of comparison. The blue triangles (case II) are results for $I_I = -0.1$ and $S_I = S/2$, leaving S_{NN} and S_{NNN} untouched (i.e., equal to S). This ultralocal magnetic dilution induces effective NN and NNN reductions in the Heisenberg couplings accelerating the rate of decrease of the critical temperatures. However, the nematic phase is still not stabilized and, thus, it does not reproduce the experimental behavior for the Co-doped parent compound. Reducing S_I to zero, as indicated by the green diamonds in the figure (case III) and keeping S_{NN} and S_{NNN} untouched, slightly increases the rate of reduction of the critical temperatures with doping and stabilizes the nematic phase only after a finite amount of doping $x \sim 10\%$ has been added but in a very narrow range of temperature. The conclusion of cases I, II, and III is that a very local description of the dopant is insufficient to reproduce experiments.

We have found that in order to generate a robust nematic phase upon doping, extended effects of magnetic dilution *must* be considered. The upside-down purple triangles (case IV) in Fig. 6 show results for $S_I = S/2$, $S_{NN} = 0.7S$, and $S_{NNN} = 0.9S$. The nematic regime is still too narrow. But the results for $S_I = 0$ with $S_{NN} = S/4$ and $S_{NNN} = S/2$ (black circles, case V), already shown in Fig. 2, indicate that increasing the strength of the extended off-diagonal disorder does induce a faster reduction of the critical temperatures and stabilizes a larger nematic region. Our computer simulations suggest that the range and strength of disorder, specifically the extended magnetic dilution, is crucial for the stabilization of the nematic phase when $T_N = T_S$ in the parent compound.

We have observed that the effect of the on-site impurity potential I_I is weak. In principle, we could have kept the overall chemical potential μ fixed and control the added electronic density n by merely adjusting the values of the impurity potential. However, this does not induce noticeable changes in the critical temperatures, due to the small overall modifications in the electronic density discussed before. This is not the manner in which doping seems to act in the real electron-doped pnictides. Thus we believe that working with a fixed value of the impurity potential and adjusting the electronic density with the overall chemical potential allows to study the effects of isotropic quenched disorder and varying electronic density in a more controlled and independent way.

Considering the negligible effect on the critical temperatures caused by pure electronic doping (clean limit) and, by extension, the on-site impurity potential, the results in Fig. 6 shed light on the case of isovalent doping in which Fe is replaced by Ru. This procedure introduces disorder but, at least nominally, no electronic doping. Experimental efforts have observed that in this case T_N and T_S still decrease with doping, despite no apparent changes in the Fermi surface, but at a slower rate than with nonisovalent doping. Moreover, the critical temperatures do not separate from each other, i.e., no nematic phase is stabilized [21]. Our results lend support to the view that the decrease of T_N and T_S observed with Ru-doping is mainly due to the magnetic dilution introduced by doping rather than by more subtle effects on the electronic density, which in turn would affect the nesting of the FS [22,23]. Experiments have determined that doped Ru is magnetic [54], which would translate to larger values of S_I, S_{NN}, and S_{NNN} in our model. In fact, the blue triangles (case II) in Fig. 6 qualitatively capture the slower decrease rate and negligible separation with impurity doping for T_N and T_S experimentally observed for Ru doping [21].

V. PROPERTIES OF THE NEMATIC PHASE

Having stabilized a robust nematic regime, let us study its properties.

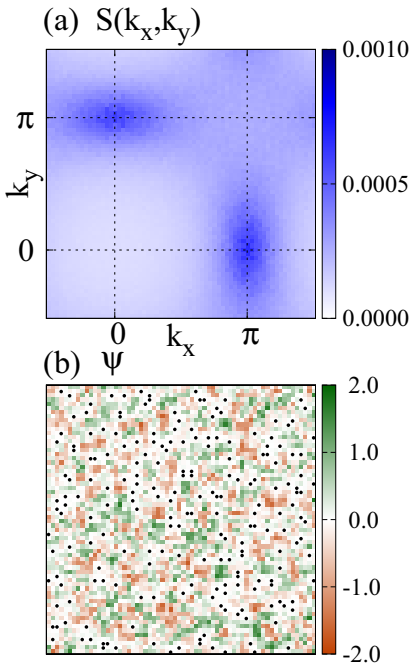

FIG. 7. (Color online) Magnetic and nematic order in the paramagnetic regime. The results are for 5% Co doping at $T = 120$ K ($T > T_S$) and using a 64×64 lattice. (a) The magnetic structure factor $S(\mathbf{k})$, showing that the wave vectors $(\pi,0)$ and $(0,\pi)$ have similar intensity. (b) Monte Carlo snapshot of the spin-nematic order parameter with approximately the same amount of positive (green) and negative (orange) clusters. The impurity sites are indicated by black dots.

A. Neutron scattering

Considering the importance of neutron scattering experiments in iron superconductors, we studied the electronic doping dependence of the magnetic structure factor $S(\mathbf{k})$ obtained from the Fourier transform of the real-space spin-spin correlation functions displayed in Fig. 4. Experiments indicate that the low-temperature magnetic phase below $T_S = T_N$ in the parent compound develops long range AFM (FM) order along the long (short) lattice constant direction in the orthorhombic lattice. This results in a sharp peak at $\mathbf{k} = (\pi,0)$ (or at $(0,\pi)$ depending on the direction of the AFM order) that forms above the small spin-gap energy [8]. More importantly for our discussion and results, upon electron doping, the $(\pi,0)$ neutron peak becomes broader along the direction transversal to the AFM order in the whole energy range [8], creating an intriguing transverselly elongated ellipse.

The results obtained numerically for 5% Co-doping are shown in Fig. 7 for $T = 120$ K ($T > T_S$), i.e., in the paramagnetic phase. In panel (a), peaks in the spin structure factor $S(\mathbf{k})$ (that represents the integral over the whole energy range of the neutron scattering results) with similar intensity at wave vectors $(\pi,0)$ and $(0,\pi)$ can be observed. Both of these peaks are elongated along the direction transversal to the corresponding spin staggered direction, in agreement with neutron scattering [8]. Our explanation for these results within our spin-fermion model is not associated with FS modifications due to electron doping, since the percentual doping is small as already discussed, but instead to the development of spin-nematic clusters, anchored by the magnetically depleted regions that form at the impurity sites. A Monte Carlo snapshot of the spin-nematic order parameter $\Psi_{\mathbf{i}}$ on a 64×64 lattice is shown in panel (b) of Fig. 7. Since $T > T_S$, patches with $(\pi,0)$ and $(0,\pi)$ nematic order, indicated with green and orange in the figure, coexist in equal proportion. By eye inspection, we believe that the $(\pi,0)$ patches tend to be slightly elongated along the x direction, while the $(0,\pi)$ patches are elongated along the y direction. This asymmetry could be the reason for the shape of the peaks in the structure factor displayed in panel (a), since elliptical peaks can be associated to different correlation lengths along the x and y axes. In Fig. 7(a), the elliptical $(\pi,0)$ peak has a correlation length larger along the x axis than the y axis.

The results corresponding to lowering the temperature into the nematic phase ($T = 95$ K) are presented in Fig. 8. In this case the subtle effects already observed in the paramagnetic phase are magnified. In panel (a), it is now clear that the peak at $(\pi,0)$ has developed a much larger weight than the peak at $(0,\pi)$, as expected. Moreover, the elongation along the transversal direction already perceived in the paramagnetic state is now better developed. The Monte Carlo snapshot of the spin-nematic order parameter in panel (b) shows that the $(\pi,0)$ (green) regions prevail over the $(0,\pi)$ (orange) regions, indicating that the symmetry under lattice rotations in the nematic phase is spontaneously broken. In addition, now the elongated shape of the $(\pi,0)$ green clusters along the AFM direction is more clear to the eye. However, despite the prevalence of $(\pi,0)$ clusters, the system does not develop long-range magnetic order [compatible with panel (b) of Fig. 4]. This is because the many $(\pi,0)$ clusters are actually "out of phase" with each other. This is understood via the visual investigation of Monte Carlo snapshots, as in panel (c) of Fig. 8, where it is shown the component of the localized spins along the easy axis, S_e, multiplied by a factor $(-1)^{\mathbf{i}_x}$ (see definition in caption; the location of the impurities is indicated with black dots). The abundant red and blue patches all indicate clusters with local $(\pi,0)$ nematic order, but shifted one with respect to the other by one lattice spacing. The very small regions with $(0,\pi)$ order, as in the orange regions of panel (b), can be barely distinguished in panel (c) with a checkerboard red/blue structure.

B. Scanning tunneling microscopy

The real-space structure of the $(\pi,0)$ nematic clusters obtained numerically, with an elongation along the x axis, can be contrasted with scanning tunneling microscopy (STM) measurements. In fact, STM studies of Co-doped $CaFe_2As_2$ at 6% doping [26,27] have already revealed the existence of unidirectional electronic nanostructures. These STM structures appear to have an average length of about eight lattice spacings along the AFM direction and it was argued that they may be possibly pinned by the Co atoms. The picture of elongated structures along the x axis is consistent with our results, as shown in panel (b) of Fig. 8. However, in our simulation the nematic structures are mainly located in between, rather than on top, the Co dopants. In our case, this arises from the fact that the effect of disorder considered here reduces the magnetic

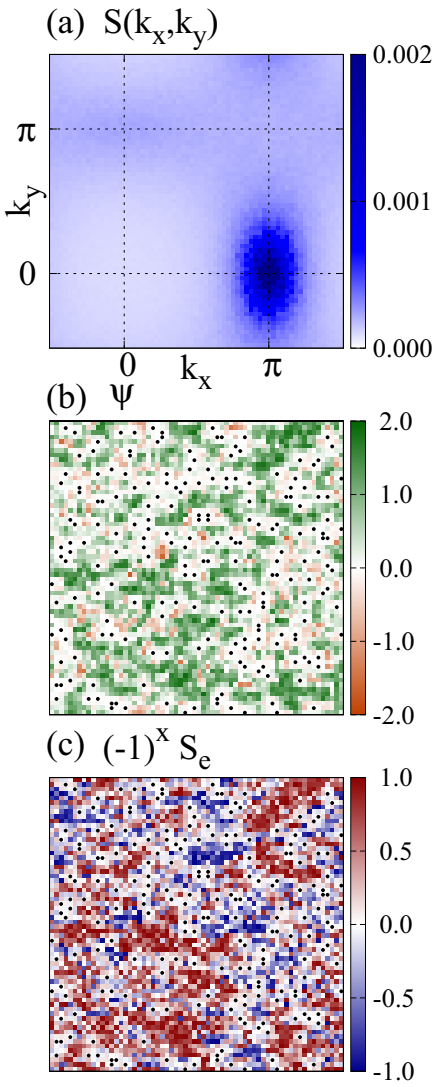

FIG. 8. (Color online) Magnetic and nematic order in the nematic regime. The results are for 5% Co-doping at $T = 95$ K ($T_N < T < T_S$) and using a 64×64 lattice. (a) The magnetic structure factor $S(\mathbf{k})$ is shown, with clear dominance of the $(\pi,0)$ state. (b) Monte Carlo snapshot of the spin-nematic order parameter. Impurity sites are indicated by black dots. A positive nematic order (green) dominates, but there are still small pockets of negative order (orange). (c) Monte Carlo snapshot displaying the on-site component along the easy axis, S_e, of the localized spin multiplied by the factor $(-1)^{\mathbf{i}_x}$, with $\mathbf{i}_x$ the x-axis component of the location of site $\mathbf{i}$. Both the dominant blue and red clusters indicate regions with *local* $(\pi,0)$ order, but shifted by one lattice spacing. This shift suppresses long-range order when averaged over the whole lattice, but short-range order remains. Impurity sites are denoted as black dots.

interactions at the Co or Cu dopant sites because they are not magnetic.

A recently discussed new perspective is that the nematic state could be a consequence of anisotropic dopant-induced scattering rather than an intrinsic nematic electronic state [25,55], by studying the anisotropy in the optical spectrum [25] and in the in-plane resistivity [55] varying Co doping in $BaFe_2As_2$. The main argument to attribute the observed anisotropies to extrinsic effects of Co doping is that the anisotropy increases with doping despite the fact that the spin order weakens and the lattice orthorhombicity diminishes. Our results, by construction, were obtained with impurity profiles that are symmetric under rotations of the lattice, so nematicity is not induced by asymmetric Co doping characteristics. However, we agree with the above described experimental observations that quenched disorder introduced by the dopants is crucial for the stabilization of the nematic phase, otherwise in the "clean limit" there is no difference between T_S and T_N as already explained.

In our simulation, the nematic phase develops because the in-plane dopants allowed the formation of cigar-shaped nematic domains. These domains have shifts in their respective AFM orders, as it can be seen in panel (c) of Fig. 8. For the 122 compounds, the dopants enhance the (weak) electronic tendency to nematicity, while according to our previous calculations [34] in the parent compound of materials in the 1111 family, such as ReFeAsO (Re = La, Nd, Sm), a small temperature range of nematicity can be provided by the coupling between the lattice and the orbital degrees of freedom. This view may be supported by studies of the phonon modes in the 1111 materials [56]. Note also that atomic-resolution variable-temperature scanning tunnelling spectroscopy experiments performed in NaFeAs, which has $T_S > T_N$, and in LiFeAs, which does not develop neither magnetic order nor a structural transition, indicate that cigar-like nematic domains develop in the nematic phase of NaFeAs regardless of the symmetry of the impurities observed in the samples [57].

VI. DISCUSSION AND CONCLUSIONS

In this publication, the effects of electron doping in materials of the 122 family, such as $BaFe_2As_2$, have been investigated via numerical studies of the spin-fermion model, including charge, orbital, magnetic, and lattice degrees of freedom. These materials are electron doped via the in-plane replacement of iron atoms by transition metal oxides, introducing disorder and dilution effects in the iron layers. The results of our study suggest that the experimentally observed reduction of the magnetic and structural transition temperatures upon doping, in such a manner that $T_N < T_S$, is primarily triggered by the influence of disorder/dilution associated with the chemical substitution of magnetic Fe atoms by nonmagnetic dopants such as Co [48] and Cu [58]. More specifically, reducing the magnitude of the localized spins at and near the dopants rapidly reduces the values of both transition critical temperatures. A "patchy" nematic phase is stabilized, which is characterized by a majority of clusters with $(\pi,0)$ order. These patches have out-of-phase magnetic order separated by nonmagnetic regions anchored by the impurities. While the tendency to nematicity is already a property of the purely electronic spin-fermion model, as already discussed in previous studies [34], the present spin-fermion model investigations suggest that for the 122 materials this fragile tendency would not materialize into a robust nematic phase without the influence of disorder/dilution. Compatible with this conclusion, $BaFe_2(As_{1-x}P_x)_2$ (considered among the "cleanest" of doped pnictides since, for example, quantum

oscillations were observed [59]) has a splitting between T_S and T_N which is very small (if any).

Note that a mere change in chemical potential to increase the electronic doping, without adding quenched disorder/dilution effects, does *not* stabilize a nematic regime in our model and induces a very small decrease in the transition temperatures. This suggests that nesting effects may not play a major role in the opening of a robust nematic window with doping in 122 materials. Our results can also rationalize the slower decrease of the critical temperatures, and lack of separation between T_N and T_S, observed upon Ru doping. In this case, experiments have shown that Ru dopants in 122 materials are magnetic [54], contrary to the nonmagnetic nature of Co and Cu dopants. Thus, in our study, the values of the Hund and Heisenberg couplings would have to be only slightly reduced at the impurity sites. As shown in Fig. 6, this will reduce the rate of decrease, as well as the separation, of T_N and T_S. The same effect may explain why $T_N = T_S$ and the decrease rate is slower in hole doped systems where the holes are introduced by replacing Ba atoms reducing the effects of disorder/dilution directly in the iron layers.

In addition, the observed clusters are elongated along the AFM direction, results compatible with observations in STM experiments. Within the spin-fermion model, the cigarlike shape of the clusters arises because the nearest-neighbor couplings are AFM and, thus, fluctuations are expected to be larger along the FM (frustrated) direction which reduces the associated correlation length. Another consequence of this behavior is the oval shape observed for the weight distribution of the magnetic structure factor around the momenta $(\pi,0)$ and $(0,\pi)$ for $T > T_N$, in agreement with the distribution observed in the electron-doped case in neutron scattering experiments.

In summary, we report the first computational study of a realistic model for pnictides that reproduces the rapid drop of T_N and T_S with the chemical replacement of Fe by transition metal elements such as Co or Cu. Since disorder and dilution affect differently T_N and T_S, a robust nematic regime is stabilized. The key ingredient is the introduction of impurity profiles that affect several neighbors around the location of the dopant. FS nesting effects were found to be too small to be the main responsible for the fast drop of critical temperatures, at least in our model. In real systems, it is conceivable that a combination of FS nesting effects and disorder/dilution effects could be simultaneously at play. Our results are also compatible with neutron scattering and also with scanning tunneling microscopy. Considering the present results for doped systems, together with the previously reported results for the parent compounds, we conclude that the spin-fermion model captures the essence of the magnetic properties of the pnictide iron superconductors.

ACKNOWLEDGMENTS

Discussions with Rafael Fernandes, Steven Kivelson, José Lorenzana, Brian Andersen, Maria Gastiasoro, Peter Hirschfeld, and Marc-Henri Julien are gratefully acknowledged. C.B. was supported by the National Science Foundation, under Grant No. DMR-1404375. E.D. and A.M. were supported by the US Department of Energy, Office of Science, Basic Energy Sciences, Materials Sciences and Engineering Division.

[1] D. C. Johnston, Adv. Phys. **59**, 803 (2010).
[2] P. J. Hirschfeld, M. M. Korshunov, and I. I. Mazin, Rep. Prog. Phys. **74**, 124508 (2011).
[3] R. M. Fernandes, A. V. Chubukov, and J. Schmalian, Nat. Phys. **10**, 97 (2014).
[4] P. Dai, J. P. Hu, and E. Dagotto, Nat. Phys. **8**, 709 (2012).
[5] E. Dagotto, Rev. Mod. Phys. **85**, 849 (2013).
[6] D. J. A. Scalapino, Rev. Mod. Phys. **84**, 1383 (2012).
[7] E. Dagotto, Rev. Mod. Phys. **66**, 763 (1994).
[8] Xianhui Chen, Pengcheng Dai, Donglai Feng, Tao Xiang, and Fu-Chun Zhang, Natl. Sci. Rev. **1**, 371 (2014).
[9] N. Ni, A. Thaler, J. Q. Yan, A. Kracher, E. Colombier, S. L. Bud'ko, P. C. Canfield, and S. T. Hannahs, Phys. Rev. B **82**, 024519 (2010).
[10] J.-H. Chu, J. G. Analytis, K. De Greve, P. L. McMahon, Z. Islam, Y. Yamamoto, and I. R. Fisher, Science **329**, 824 (2010).
[11] J.-H. Chu, H.-H. Kuo, J. G. Analytis, and I. R. Fisher, Science **337**, 710 (2012).
[12] H.-H. Kuo, Jiun-Haw Chu, Scott C. Riggs, Leo Yu, Peter L. McMahon, Kristiaan De Greve, Yoshihisa Yamamoto, James G. Analytis, and Ian R. Fisher, Phys. Rev. B **84**, 054540 (2011).
[13] I. R. Fisher, L. Degiorgi, and Z. X. Shen, Rep. Prog. Phys. **74**, 124506 (2011).
[14] R. M. Fernandes, L. H. VanBebber, S. Bhattacharya, P. Chandra, V. Keppens, D. Mandrus, M. A. McGuire, B. C. Sales, A. S. Sefat, and J. Schmalian, Phys. Rev. Lett. **105**, 157003 (2010).
[15] R. M. Fernandes, A. V. Chubukov, J. Knolle, I. Eremin, and J. Schmalian, Phys. Rev. B **85**, 024534 (2012).
[16] R. M. Fernandes and J. Schmalian, Supercond. Sci. Technol. **25**, 084005 (2012).
[17] H. Kontani, Y. Inoue, T. Saito, Y. Yamakawa, and S. Onari, Solid State Comm. **152**, 718 (2012).
[18] Q. Si and E. Abrahams, Phys. Rev. Lett. **101**, 076401 (2008).
[19] C. Fang, H. Yao, W.-F. Tsai, J. P. Hu, and S.A. Kivelson, Phys. Rev. B **77**, 224509 (2008).
[20] C. Xu, M. Müller, and S. Sachdev, Phys. Rev. B **78**, 020501(R) (2008).
[21] F. Rullier-Albenque, D. Colson, A. Forget, P. Thuéry, and S. Poissonnet, Phys. Rev. B **81**, 224503 (2010).
[22] H. Wadati, I. Elfimov, and G. A. Sawatzky, Phys. Rev. Lett. **105**, 157004 (2010).
[23] Limin Wang, Tom Berlijn, Yan Wang, Chia-Hui Lin, P. J. Hirschfeld, and Wei Ku, Phys. Rev. Lett. **110**, 037001 (2013).
[24] The upper critical temperatures T_N and T_S are mainly regulated by x, but there are still differences between different transition metals. For instance, to scale almost exactly these critical temperatures for the cases of Ni and Co, a factor 1.6 is needed to relate the dopant concentrations, as shown in H.-H. Kuo and I. R. Fisher, Phys. Rev. Lett. **112**, 227001 (2014). In that publication, it was also shown that the strain-induced resistivity anisotropy in the tetragonal state is independent of disorder. We will address this subject in future publications.

[25] M. Nakajima, S. Ishida, Y. Tomioka, K. Kihou, C. H. Lee, A. Iyo, T. Ito, T. Kakeshita, H. Eisaki, and S. Uchida, Phys. Rev. Lett. **109**, 217003 (2012).
[26] T. M. Chuang, M. P. Allan, Jinho Lee, Yang Xie, Ni Ni, S. L. Bud'ko, G. S. Boebinger, P. C. Canfield, and J. C. Davis, Science **327**, 181 (2010).
[27] M. P. Allan, T.-M. Chuang, F. Massee, Yang Xie, Ni Ni, S. L. Bud'ko, G. S. Boebinger, Q. Wang, D. S. Dessau, P. C. Canfield, M. S. Golden, and J. C. Davis, Nat. Phys. **9**, 220 (2013).
[28] T. Iye, M.-H. Julien, H. Mayaffre, M. Horvatić, C. Berthier, K. Ishida, H. Ikeda, S. Kasahara, T. Shibauchi, and Y. Matsuda, J. Phys. Soc. Jpn. **84**, 043705 (2015).
[29] The importance of disorder near a nematic quantum critical point has been recently remarked in Hsueh-Hui Kuo, Jiun-Haw Chu, Steven A. Kivelson, and Ian R. Fisher, arXiv:1503.00402.
[30] Quenched disorder has interesting consequences also in other contexts where nematicity plays an important role as shown in L. Nie, G. Tarjus, and S. A. Kivelson, Proc. Natl. Acad. Sci. USA **111**, 7980 (2014) in the pseudogap regime of the cuprates.
[31] W. Lv, F. Krüger, and P. Phillips, Phys. Rev. B **82**, 045125 (2010).
[32] W.-G. Yin, C.-C. Lee, and W. Ku, Phys. Rev. Lett. **105**, 107004 (2010).
[33] S. Liang, G. Alvarez, C. Sen, A. Moreo, and E. Dagotto, Phys. Rev. Lett. **109**, 047001 (2012).
[34] Shuhua Liang, Adriana Moreo, and Elbio Dagotto, Phys. Rev. Lett. **111**, 047004 (2013).
[35] H. Gretarsson, A. Lupascu, J. Kim, D. Casa, T. Gog, W. Wu, S. R. Julian, Z. J. Xu, J. S. Wen, G. D. Gu, R. H. Yuan, Z. G. Chen, N.-L. Wang, S. Khim, K. H. Kim, M. Ishikado, I. Jarrige, S. Shamoto, J.-H. Chu, I. R. Fisher, and Y.-J. Kim, Phys. Rev. B **84**, 100509(R) (2011).
[36] F. Bondino, E. Magnano, M. Malvestuto, F. Parmigiani, M. A. McGuire, A. S. Sefat, B. C. Sales, R. Jin, D. Mandrus, E. W. Plummer, D. J. Singh, and N. Mannella, Phys. Rev. Lett. **101**, 267001 (2008).
[37] M. Daghofer, A. Nicholson, A. Moreo, and E. Dagotto, Phys. Rev. B **81**, 014511 (2010).
[38] C. de la Cruz, Q. Huang, J. W. Lynn, Jiying Li, W. Ratcliff II, J. L. Zarestky, H. A. Mook, G. F. Chen, J. L. Luo, N. L. Wang, and Pengcheng Dai, Nature (London) **453**, 899 (2008).
[39] J. Schmiedt, P. M. R. Brydon, and C. Timm, Phys. Rev. B **85**, 214425 (2012).
[40] Maria N. Gastiasoro, P. J. Hirschfeld, and B. M. Andersen, Phys. Rev. B **89**, 100502(R) (2014); M. N. Gastiasoro, I. Paul, Y. Wang, P. J. Hirschfeld, and B. M. Andersen, Phys. Rev. Lett. **113**, 127001 (2014); Y. Wang, M. N. Gastiasoro, B. M. Andersen, M. Tomic, H. O. Jeschke, R. Valentí, I. Paul, and P. J. Hirschfeld, *ibid.* **114**, 097003 (2015).
[41] Shuhua Liang, Anamitra Mukherjee, Niravkumar D. Patel, Christopher B. Bishop, Elbio Dagotto, and Adriana Moreo, Phys. Rev. B **90**, 184507 (2014).
[42] J. L. Niedziela, D. Parshall, K. A. Lokshin, A. S. Sefat, A. Alatas, and T. Egami, Phys. Rev. B **84**, 224305 (2011).
[43] M. G. Vavilov and A. V. Chubukov, Phys. Rev. B **84**, 214521 (2011).
[44] R. M. Fernandes, M. G. Vavilov, and A. V. Chubukov, Phys. Rev. B **85**, 140512(R) (2012).
[45] The magnitude of the localized spins is set to $S_{\mathbf{i}} = 1$ since the actual value is absorbed into the Hamiltonian parameters. For example if $S_{\mathbf{i}}$ is changed to a value S' the Hamiltonian parameters related to the site $\mathbf{i}$ change in the following way: $J_{\mathrm{H},\mathbf{i}} = S' J_{\mathrm{H}}$, $g_{\mathbf{i}} = S' g$, $J_{\mathrm{NN},\mathbf{i}} = S' J_{\mathrm{NN}}$, and $J_{\mathrm{NNN},\mathbf{i}} = S' J_{\mathrm{NNN}}$.
[46] The spin in H_{SL} is only the localized spin for computational simplicity.
[47] E. Dagotto, T. Hotta, and A. Moreo, Phys. Rep. **344**, 1 (2001).
[48] A. S. Sefat, D. J. Singh, R. Jin, M. A. McGuire, B. C. Sales, and D. Mandrus, Phys. Rev. B **79**, 024512 (2009).
[49] S. Kumar and P. Majumdar, Eur. Phys. J. B **50**, 571 (2006).
[50] J. Salafranca, G. Alvarez, and E. Dagotto, Phys. Rev. B **80**, 155133 (2009).
[51] M. Capati, M. Grilli, and J. Lorenzana, Phys. Rev. B **84**, 214520 (2011).
[52] Smaller, and for some points, larger systems with up to 96×96 sites where studied to monitor that finite size effects are very small in the 64×64 clusters used to obtain the results presented here.
[53] The value was chosen to simulate the on-site potential reduction with respect to the background Fe potential observed experimentally. See G. Levy, R. Sutarto, D. Chevrier, T. Regier, R. Blyth, J. Geck, S. Wurmehl, L. Harnagea, H. Wadati, T. Mizokawa, I. S. Elfimov, A. Damascelli, and G. A. Sawatzky, Phys. Rev. Lett. **109**, 077001 (2012).
[54] M. G. Kim, J. Soh, J. Lang, M. P. M. Dean, A. Thaler, S. L. Bud'ko, P. C. Canfield, E. Bourret-Courchesne, A. Kreyssig, A. I. Goldman, and R. J. Birgeneau, Phys. Rev. B **88**, 014424 (2013).
[55] S. Ishida, M. Nakajima, T. Liang, K. Kihou, C. H. Lee, A. Iyo, H. Eisaki, T. Kakeshita, Y. Tomioka, T. Ito, and S. Uchida, Phys. Rev. Lett. **110**, 207001 (2013).
[56] T. Dong, Z. G. Chen, R. H. Yuan, B. F. Hu, B. Cheng, and N. L. Wang, Phys. Rev. B **82**, 054522 (2010).
[57] E. P. Rosenthal, E. F. Andrade, C. J. Arguello, R. M. Fernandes, L. Y. Xing, X. C. Wang, C. Q. Jin, A. J. Millis, and A. N. Pasupathy, Nat. Phys. **10**, 225 (2014).
[58] D. J. Singh, Phys. Rev. B **79**, 153102 (2009).
[59] J. G. Analytis, J.-H. Chu, R. D. McDonald, S. C. Riggs, and I. R. Fisher, Phys. Rev. Lett. **105**, 207004 (2010).